
AI translation · View original & related papers at
chinarxiv.org/items/chinaxiv-202201.00108

Distribution Characteristics and Genesis of Fluoride in Groundwater in the Hotan Region (Post-print)

Authors: Shi Wenwen

Date: 2022-01-26T18:10:10+00:00

Abstract

The Hotan region is located in the southwestern part of Xinjiang, characterized by an arid climate and scarce precipitation. Groundwater serves as an important drinking water source in the Hotan region, making the investigation of fluoride distribution and genesis in groundwater of great significance to human health. Based on 217 sets of shallow groundwater quality test results from the Hotan region, Xinjiang, spanning 2002–2018, this study employs GIS technology, mathematical statistics, Gibbs diagrams, and hydrogeochemical simulation methods to investigate the spatiotemporal distribution characteristics and formation processes of fluoride in shallow groundwater in the Hotan region. The results indicate that fluoride concentrations in groundwater in the study area range from 0.05~16.95 mg·L⁻¹, with a mean value of 1.38 mg·L⁻¹, and an exceedance rate as high as 36.1%. In the horizontal direction, high-fluoride groundwater is sporadically distributed in small areas; in the vertical direction, fluoride content exhibits a decreasing trend with increasing well depth. Groundwater fluoride content shows an increasing trend over time. Fluoride in groundwater is related to the hydrochemical environment, wherein high alkalinity and HCO₃ concentration increase the solubility of fluoride in groundwater. In addition to hydrogeological conditions and the hydrochemical environment, intense evaporation and concentration, water–rock interaction, and cation exchange adsorption control the migration and enrichment processes of fluoride in the groundwater system.

Full Text

Distribution Characteristics and Formation Process of Fluorine in Groundwater in Hotan Prefecture

SHI Wenwen^{1,2,3}, ZHOU Jinlong^{1,2,3}, ZENG Yanyan^{1,2,3}, SUN Ying^{1,2,3}

¹College of Water Conservancy and Civil Engineering, Xinjiang Agricultural University, Urumqi 830052, Xinjiang, China

²Xinjiang Hydrology and Water Resources Engineering Research Center, Urumqi 830052, Xinjiang, China

³Xinjiang Key Laboratory of Hydraulic Engineering Security and Water Disasters Prevention, Urumqi 830052, Xinjiang, China

Abstract: Hotan Prefecture is located in southwestern Xinjiang and is characterized by a dry climate with sparse rainfall. Groundwater serves as a crucial drinking water source in this region, making it essential to investigate the distribution and genesis of fluorine in groundwater for public health protection. Based on 217 sets of shallow groundwater quality test results from Hotan Prefecture, Xinjiang, collected between 2002 and 2018, this study examines the spatiotemporal distribution characteristics and formation mechanisms of fluoride in shallow groundwater using GIS technology, mathematical statistics, Gibbs diagrams, and hydrogeochemical simulations. The results indicate that fluoride concentrations in groundwater range from $0.05\text{--}16.95\text{ mg}\cdot\text{L}^{-1}$, with a mean value of $1.38\text{ mg}\cdot\text{L}^{-1}$, and an exceedance rate of 36.1% relative to the national drinking water standard. Horizontally, high-fluoride groundwater occurs sporadically in small patches; vertically, fluoride content decreases with increasing well depth. Over time, groundwater fluoride concentrations show an increasing trend. Fluoride exhibits a clear relationship with the hydrochemical environment, wherein high alkalinity and HCO_3^- concentrations enhance fluoride solubility. In addition to hydrogeological conditions and the hydrochemical environment, strong evaporation concentration, water-rock interactions, and cation exchange adsorption collectively control fluoride migration and enrichment in the groundwater system.

Keywords: Hotan Prefecture; high-fluoride groundwater; cause analysis; hydrogeochemical model

1.1 Study Area Overview

Hotan Prefecture is situated in southwestern Xinjiang, bordering Bayingolin Mongol Autonomous Prefecture to the east, Kashgar Prefecture to the west, the northern Tibetan Plateau across the Kunlun Mountains to the south, and extending into the hinterland of the Taklamakan Desert to the north. The region spans $34^{\circ}33\text{--}39^{\circ}66\text{ N}$ and $77^{\circ}39\text{--}84^{\circ}91\text{ E}$, covering a total area of

$24.78 \times 10^4 \text{ km}^2$, which accounts for 15% of Xinjiang's land area. The area experiences frequent sandstorms and floating dust in spring, with hot and dry summers, characteristic of a temperate continental arid climate. Annual precipitation ranges from 35.6 mm in the northern desert area to 120 mm in the southern mountainous region, while annual evaporation varies between 2159~3137 mm. The dryness index exceeds 20, and temperatures decrease from 12.5 °C in the southern mountains to 9.4 °C in the northern desert.

Geologically, the central plain of Hotan Prefecture spans two tectonic units: the Southeast Depression and the Hotan Depression, primarily exposing Neogene and Quaternary strata. The depressions contain massive Quaternary loose deposits that provide excellent aquifer storage space. In the upper alluvial-proluvial plain, the sediments consist of sandy gravel and cobble, hosting unconfined groundwater with abundant yields. The middle section comprises sandy gravel and coarse sand containing alluvial-proluvial pore water, while the lower section consists of fine sand and silt with multi-layer unconfined-confined groundwater, mainly distributed in the front edge of the Keriya River alluvial-proluvial plain with moderate water yields.

Groundwater recharge in the southern mountainous and low hilly areas of Hotan Prefecture is minimal from precipitation infiltration, primarily receiving contributions from bedrock fissure water. The piedmont plain area is mainly recharged by surface water leakage, while the desert region, being extremely arid with intense evaporation, relies solely on subsurface flow from upstream areas. The general groundwater flow direction is from south to north, with the hydraulic gradient gradually decreasing and flow velocities slowing. Evapotranspiration from phreatic water and artificial extraction constitute the primary discharge mechanisms.

1.2 Groundwater Sample Collection and Testing

Between 2002 and 2018, 217 shallow groundwater samples were collected in Hotan Prefecture, including 126 unconfined water samples and 91 shallow confined water samples. The sampling density was 1.0~1.6 sites per 100 km², with the 2018 sampling campaign covering an area of 12,937 km². This density fully meets the requirement of 1.0~1.6 sites per 100 km² for groundwater quality monitoring in over-exploited inland basin plain areas as specified in the *Groundwater Monitoring Standard* (SL183-2005). Sample collection, preservation, and submission strictly followed the *Technical Specifications for Groundwater Environmental Monitoring* (HJ/T164-2004).

The 2018 water samples were analyzed at the laboratory of the Second Hydrogeological and Engineering Geological Brigade of the Xinjiang Bureau of Geology and Mineral Resources, while the 2002 samples were tested at the Mineral Water Testing Center of the Institute of Hydrogeology and Environmental Geology, Chinese Academy of Geological Sciences. Analysis included K⁺, Na⁺,

Ca^{2+} , Mg^{2+} , Cl^- , SO_4^{2-} , HCO_3^- , total hardness (TH), total dissolved solids (TDS), pH, and fluoride concentration. Data reliability was verified using the charge balance error percentage method for anion-cation balance, with all samples showing errors $|\text{CBE}| < 5\%$, indicating high data quality.

Given the larger dataset from 2018, subsequent analyses primarily utilize 2018 data, with same-location data used to characterize interannual fluoride variation. Data organization and statistical analysis were performed using Excel, while sampling point distribution maps and fluoride concentration spatial distribution maps were generated using Surfer. Piper diagrams were created using Grapher software. Correlation analysis between fluoride and various ions was conducted using Origin, and saturation indices were calculated and inverse hydrogeochemical modeling performed using Phreeqc.

2.1 Groundwater Chemical Characteristics and Fluoride Content Levels

Based on 2018 data for major hydrochemical parameters in Hotan Prefecture groundwater (Table 1), pH ranges from 7.01~9.63, indicating weakly alkaline conditions. TDS varies from $414.91\text{--}41282.73 \text{ mg} \cdot \text{L}^{-1}$, classifying the water as primarily brackish. Cation mass concentrations follow the order $\text{Na}^+ > \text{Ca}^{2+} > \text{Mg}^{2+} > \text{K}^+$, while anion mass concentrations show $\text{Cl}^- > \text{SO}_4^{2-} > \text{HCO}_3^-$. Except for Na^+ and Cl^- , other ions exhibit large variation coefficients, indicating extremely uneven spatial distribution.

The Piper trilinear diagram (Figure 2) reveals that both unconfined and shallow confined water samples plot in the lower right corner for cations, dominated by Na^+ and Ca^{2+} , while anions cluster in the middle-right portion, primarily as $\text{Cl} \cdot \text{SO}_4$. This indicates that shallow groundwater in the study area is mainly influenced by evaporite weathering. Unconfined water chemistry types are predominantly $\text{Cl} \cdot \text{SO}_4\text{-Na} \cdot \text{Ca}$ and $\text{Cl} \cdot \text{SO}_4\text{-Na} \cdot \text{Mg}$, while shallow confined water is primarily $\text{SO}_4\text{-Na} \cdot \text{Mg}$ and Cl-Na .

Fluoride concentrations in Hotan Prefecture groundwater range from 0.05~16.95 $\text{mg} \cdot \text{L}^{-1}$, with a mean of $1.38 \text{ mg} \cdot \text{L}^{-1}$, exceeding the $1.0 \text{ mg} \cdot \text{L}^{-1}$ limit in China's *Standards for Drinking Water Quality*. The variation coefficient of 164.7% indicates highly uneven distribution. A total of 43 samples (36.1%) exceed the fluoride standard. As shown in Table 2, unconfined $\text{HCO}_3 \cdot \text{Cl} \cdot \text{SO}_4\text{-Na} \cdot \text{Ca}$ type water has the lowest mean fluoride content ($0.59 \text{ mg} \cdot \text{L}^{-1}$), while $\text{Cl} \cdot \text{SO}_4\text{-Na} \cdot \text{Ca}$ type has the highest ($2.60 \text{ mg} \cdot \text{L}^{-1}$). For confined water, $\text{SO}_4\text{-Na} \cdot \text{Mg}$ type shows the lowest mean fluoride ($0.68 \text{ mg} \cdot \text{L}^{-1}$), while $\text{Cl} \cdot \text{SO}_4\text{-Na} \cdot \text{Mg}$ type has the highest ($6.68 \text{ mg} \cdot \text{L}^{-1}$). High-fluoride water is characterized by higher mineralization and weak acid anion concentrations exceeding strong acid anions, whereas confined water shows the opposite pattern. This demonstrates that fluoride migration and enrichment are influenced by multiple factors, primarily evaporation concentration and ion exchange adsorption.

2.2.1 Horizontal Distribution

The spatial distribution map of fluoride content in 2018 (Figure 3) shows that groundwater with fluoride $<1.0 \text{ mg} \cdot \text{L}^{-1}$ dominates the study area, with high-fluoride groundwater distributed sporadically in small patches. High-fluoride zones in unconfined water occur in every county, but Minfeng, Yutian, Lopu, Hotan City, and Moyu counties exhibit particularly high concentrations over larger areas. Groundwater with fluoride $<1.0 \text{ mg} \cdot \text{L}^{-1}$ is mainly found near southern river outlets where aquifer media have relatively large particles, groundwater flow is rapid, and the area is controlled by geomorphic lithofacies belts with deep water tables and minimal evaporation. Additionally, surface water recharge (fluoride content $0.5\text{--}0.7 \text{ mg} \cdot \text{L}^{-1}$) dilutes fluoride concentrations in these areas. Shallow confined water high-fluoride zones are primarily distributed in Minfeng County, with minor distribution in Yutian County. Overall, fluoride content is similar across counties, with only Minfeng showing notably elevated levels.

2.2.2 Vertical Distribution

Analysis of 2018 data reveals a correlation between fluoride content and well depth (Figure 4). Fluoride concentrations initially increase then decrease with depth, with high-fluoride groundwater mainly occurring within 10~40 m depth, though some high-fluoride points also appear at 40~100 m depth. This indicates hydraulic connectivity between aquifers, likely due to leakage from overlying aquifers and lateral recharge from mountain front precipitation.

2.3 Interannual Variation Characteristics

To characterize interannual fluoride variation, seven groups of same-location unconfined water samples were compared (Table 4). Results show that five groups exhibit increasing fluoride trends, with three showing substantial increases and two exceeding $1.0 \text{ mg} \cdot \text{L}^{-1}$. One group shows decreasing fluoride content, while another demonstrates an initial increase followed by decrease, indicating fluoride contamination risks in some areas.

2.4 Relationship Between Fluorine and Hydrochemical Environment

Fluoride content is closely related to the hydrochemical environment, with different chemical components influencing fluoride occurrence and evolution. Pearson correlation analysis (Table 5) shows fluoride is significantly correlated with Na^+ ,

HCO_3^- , TDS, and pH at the 0.01 level (two-tailed), and with Ca^{2+} and Mg^{2+} at the 0.05 level. Research indicates that high alkalinity and HCO_3^- concentrations increase fluoride solubility. In Hotan Prefecture, high-fluoride groundwater has pH values of 7.01~9.63, indicating neutral to alkaline conditions where fluoride concentrations increase with pH. Additionally, rising HCO_3^- concentrations enhance ionic strength, further increasing fluoride solubility. The positive correlation between fluoride and TDS is significant when $\text{TDS} < 4000 \text{ mg} \cdot \text{L}^{-1}$, but becomes less pronounced at higher concentrations, suggesting salt effects influence fluoride behavior within certain ranges.

The relationship between fluoride and Ca^{2+} varies regionally. In this study area, the correlation is not significant, indicating other factors or processes may disrupt the typical inverse relationship. When Ca^{2+} concentrations are high, fluoride concentrations are also elevated, suggesting additional mechanisms facilitate fluoride entry into groundwater.

2.5.1 Evaporation Concentration Effect

Gibbs diagrams semi-quantitatively illustrate groundwater ion characteristics and controlling mechanisms. Figure 6 shows that Hotan Prefecture groundwater samples have $\text{TDS} > 100 \text{ mg} \cdot \text{L}^{-1}$ and plot primarily in the rock weathering and evaporation concentration zones, with no samples in the atmospheric precipitation zone. This indicates that rock-water interactions and evaporation concentration dominate groundwater chemistry, consistent with the region's arid climate.

2.5.2 Cation Exchange Adsorption

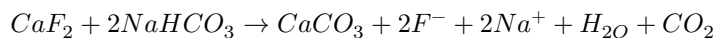
Cation exchange alters major cation concentrations and promotes fluoride release from fluorine-bearing minerals into groundwater. This process can be evaluated using the chlor-alkali index (CAI). If both CAI-1 and CAI-2 are positive, Na^+ in groundwater exchanges with Ca^{2+} and Mg^{2+} in the aquifer; if both are negative, the reverse exchange occurs; values near zero indicate minimal exchange. Larger absolute values indicate stronger cation exchange.

Figure 7 shows most samples have negative CAI values with large absolute magnitudes, indicating Na^+ in groundwater exchanges with Ca^{2+} and Mg^{2+} in the aquifer. This process facilitates fluoride dissolution, consistent with the weak negative correlation between Ca^{2+} and fluoride.

2.6.1 Component Distribution Model

Component distribution models, also known as ion complexation models, investigate the thermodynamic controls on fluoride concentrations and calculate species equilibrium states through mineral saturation indices (SI). When $SI > 0$, minerals are supersaturated; when $SI < 0$, they are undersaturated; and when $SI = 0$, they are at equilibrium.

Figure 8 shows most groundwater samples plot in the saturation zones for dolomite and calcite, indicating effective carbonate mineral interactions. Most samples are supersaturated with respect to calcite (99.2%) and dolomite (98.3%), showing precipitation potential that favors fluoride enrichment. Conversely, 99.2% of samples are undersaturated with respect to gypsum, allowing fluoride to migrate and accumulate under suitable conditions. Although fluorite has low solubility, calcite precipitation drives fluorite dissolution (Equation 1), consistent with previous research.



2.6.2 Reverse Path Model

Using ArcGIS to visualize fluoride spatial distribution (Figure 3), with color intensity indicating fluoride concentration, and considering the general south-to-north groundwater flow direction, two simulation paths were established (Figure 3). Hydrochemical data for points along these paths are presented in Table 6. Common mineral phases including anhydrite, calcite, dolomite, fluorite, gypsum, halite, and cation exchange were selected as potential reaction phases for inverse modeling.

Reverse hydrogeochemical modeling results (Table 7) show that for unconfined water along Path I, anhydrite and calcite precipitate while other minerals dissolve. Dolomite dissolution increases Ca^{2+} and Mg^{2+} concentrations, fluorite dissolution releases fluoride, and gypsum dissolution enhances Ca^{2+} solubility. Shallow confined water along Path II shows similar patterns, with mineral dissolution increasing Ca^{2+} , Mg^{2+} , and HCO_3^- concentrations. Overall, groundwater evolution in the study area is dominated by anhydrite and calcite precipitation coupled with dissolution of dolomite, fluorite, and gypsum. The discrepancy between dolomite dissolution in the model and saturation index calculations suggesting saturation may result from atmospheric CO_2 dissolution during groundwater flow and precipitation lag effects.

3 Conclusions

1. Groundwater in Hotan Prefecture is weakly alkaline brackish water. Unconfined water chemistry types are primarily $\text{Cl} \cdot \text{SO}_4\text{-Na} \cdot \text{Ca}$ and $\text{Cl} \cdot \text{SO}_4\text{-Na} \cdot \text{Mg}$, while shallow confined water types are mainly $\text{SO}_4\text{-Na} \cdot \text{Mg}$ and Cl-Na . Fluoride concentrations range from $0.05\text{--}16.95 \text{ mg} \cdot \text{L}^{-1}$, averaging $1.38 \text{ mg} \cdot \text{L}^{-1}$, with an exceedance rate of 36.1%.
2. Fluoride distribution is controlled by groundwater recharge, flow, and discharge conditions. High-fluoride groundwater occurs sporadically in small patches in relatively low-lying areas of the central plain. Vertically, fluoride content decreases with increasing well depth, with high-fluoride water most likely occurring within 40 m depth. Fluoride concentrations show an increasing trend over time.
3. The relationship between fluoride and the hydrochemical environment demonstrates that high pH and HCO_3^- concentrations increase fluoride solubility. The region's arid climate, strong evaporation concentration, cation exchange adsorption, and water-rock interactions leading to mineral dissolution or precipitation collectively control fluoride enrichment in groundwater.

References

- [1] Tu Chenglong, He Lingling, Cui Lifeng, et al. Environmental and geochemical behaviors of fluorine and its impacts on ecological environment[J]. Chinese Journal of Applied Ecology, 2019, 30(1): 21-29.
- [2] Fordyce F M, Vrana K, Zhovinsky E, et al. A health risk assessment for fluoride in Central Europe[J]. Environmental Geochemistry and Health, 2007, 29(2): 83-102.
- [3] Ali S, Thakur S K, Sarkar A, et al. Worldwide contamination of water by fluoride[J]. Environmental Chemistry Letters, 2016, 14(3): 291-315.
- [4] Lyu Xiaoli, Liu Jingtao, Zhou Bing, et al. Distribution characteristics and enrichment mechanism of fluoride in the shallow aquifer of the Tacheng Basin[J]. Earth Science Frontiers, 2021, 28(2): 426-436.
- [5] Li Qiao, Jia Ruiliang, Zhou Jinlong, et al. Analysis of chemical characteristics of high fluoride groundwater in Aksu prefecture, Xinjiang[J]. Journal of Arid Land Resources and Environment, 2013, 27(12): 87-92.
- [6] Luan Fengjiao, Zhou Jinlong, Zeng Yanyan, et al. Distribution characteristics and enrichment factors of fluorine in groundwater in typical areas of southern Xinjiang[J]. Environmental Chemistry, 2016, 35(6): 1203-1211.
- [7] Li Ling, Zhou Jinling, Qi Wanqiu, et al. Distribution and formation process of fluorine in groundwater in oasis area of Hotan River Basin[J]. Journal of Arid

Land Resources and Environment, 2019, 33(1): 112-118.

- [8] Zhang Jie, Zhou Jinlong, Nai Weihua, et al. Characteristics of high fluoride groundwater in plain of Yarkant river basin in Xinjiang[J]. Journal of Arid Land Resources and Environment, 2020, 34(4): 100-106.
- [9] Sun Qian, Aliya Baidourela. Mathematical fitting of influencing factors and measured groundwater level: Take Keriya River Basin in Hotan area as an example[J]. Progress in Geography, 2018, 37(7): 912-922.
- [10] Liang Bing. The Application of Hydrochemical Characteristics on Transform Relationship Between Surface Water and Groundwater in the Hotan River Basin[D]. Urumqi: Xinjiang University, 2018.
- [11] Ma Jinzhu. Groundwater resources and its sustainable development in Hotan Region, Xingjiang[J]. Journal of Desert Research, 2002, 22(3): 41-47.
- [12] Zeng Yanyan, Wu Jinrong, Zhou Jinlong, et al. Assessment of groundwater quality and pollution in Hotan Region of Xinjiang[J]. Yellow River, 2015, 37(7): 79-81.
- [13] Wu Chu, Wu Xiong, Zhang Yanshuai, et al. Distribution characteristics and genesis of fluoride groundwater in the Niuxin Mountain, Qinhuangdao[J]. Earth Science Frontiers, 2018, 25(4): 307-315.
- [14] Saxena V, Ahmed S. Dissolution of fluoride in groundwater: A water-rock interaction study[J]. Environmental Geology, 2001, 40(9): 1084-1087.
- [15] Rafique T, Naseem S, Usmani T H, et al. Geochemical factors controlling the occurrence of high fluoride groundwater in the Nagar Parkar area, Sindh, Pakistan[J]. Journal of Hazardous Materials, 2009, 171(1-3): 424-430.
- [16] Wang Lei, Dong Shaogang, Wang Xuexin, et al. Hydrogeochemical characteristics and origin of Shenquan in Tuoketuo County, Inner Mongolia[J]. Arid Zone Research, 2020, 37(5): 1140-1147.
- [17] Yan J, Chen J, Zhang W, et al. Determining fluoride distribution and influencing factors in groundwater in Songyuan, Northeast China, using hydrochemical and isotopic methods[J]. Journal of Geochemical Exploration, 2020, 217: 106605.
- [18] Keesari T, Sinha U K, Deodhar A, et al. High fluoride in groundwater of an industrialized area of Eastern India (Odisha): Inferences from geochemical and isotopic investigation[J]. Environmental Earth Sciences, 2016, 75(14): 1-17.
- [19] Gibbs R J. Mechanisms Controlling World Water Chemistry[J]. Science, 1970, 170(3962): 1088-1090.
- [20] Rashid A, Guan D X, Farooqi A, et al. Fluoride prevalence in groundwater around a fluorite mining area in the flood plain of the River Swat, Pakistan[J]. Science of The Total Environment, 2018, 635: 203-215.

[21] Wu C, Wu X, Qian C, et al. Hydrogeochemistry and groundwater quality assessment of high fluoride levels in the Yanchi endorheic region, northwest China[J]. *Applied Geochemistry*, 2018, 98: 404-417.

[22] Su C, Wang Y, Xie X, et al. An isotope hydrochemical approach to understand fluoride release into groundwaters of the Datong Basin, Northern China[J]. *Environmental Science Process and Impacts*, 2015, 17(4): 791-801.

[23] Su C, Wang Y, Xie X, et al. Aqueous geochemistry of high fluoride groundwater in Datong Basin, Northern China[J]. *Journal of Geochemical Exploration*, 2013, 135(1): 79-92.

[24] Mao Meng, Zhu Xueqin. Chemical characteristics of groundwater in Xuanhua Basin and assessment of irrigation applicability[J]. *Journal of Arid Land Resources and Environment*, 2020, 34(7): 142-149.

[25] Liu Hai, Kang Bo, Shen Junhui. Formation of groundwater based on inverse geochemical modeling: A case study from the Sixian County, Anhui Province[J]. *Geoscience*, 2019, 33(2): 440-450.

Figures

Source: ChinaXiv –Machine translation. Verify with original.

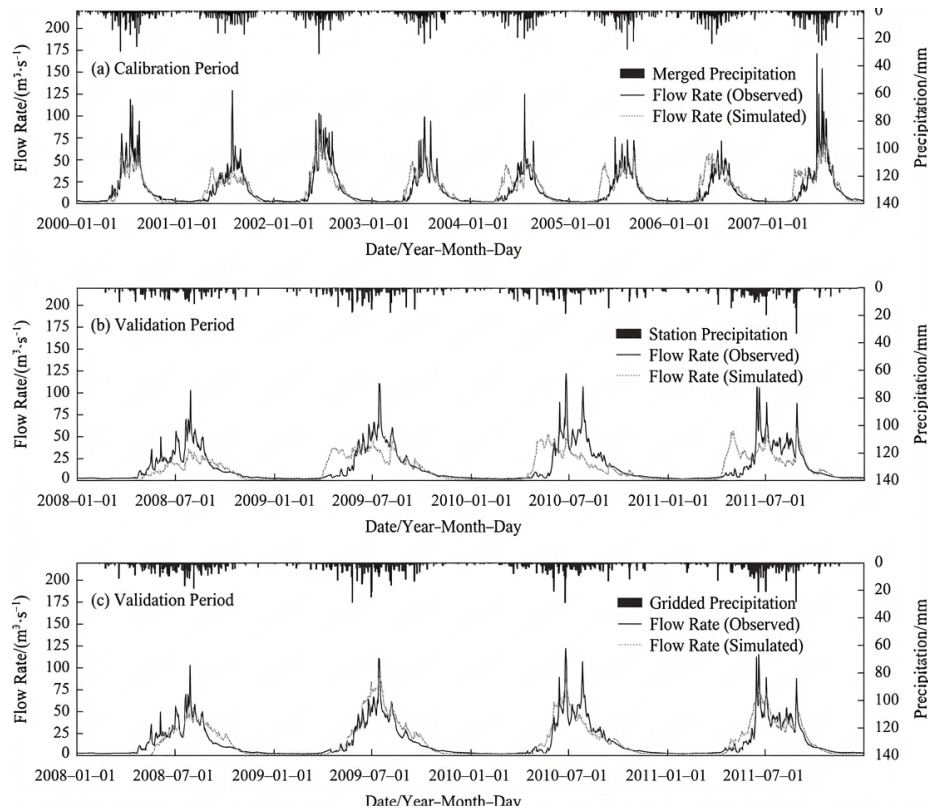


Figure 1: Figure 3

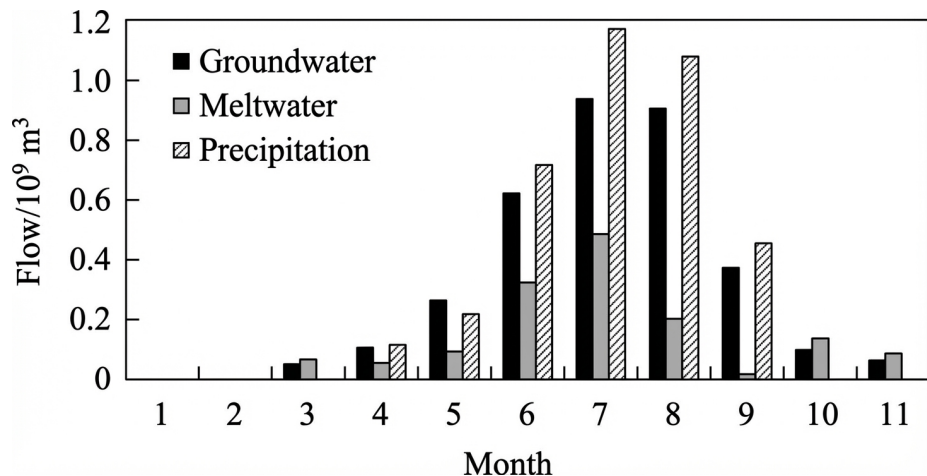


Figure 2: Figure 7

